electronics

MDPI

Article

Numerical Evaluation of Sparse Residual Correction for Joint Luminance and Chromaticity Calibration in Mini-LED Displays

Jinhuan Yu [1,2,3], Xifeng Zheng [1,2,3], Ran Zhan [1,2], Yufeng Chen [1,2,3], Yang Wang [1,2,3,*], Hui Cao [3], Yu Chen [1,2,3] and Xinyue Mao [1,3]

[1] Changchun Institute of Optics, Fine Mechanics and Physics, Chinese Academy of Sciences, Changchun 130033, China; yujinhuan24@mails.ucas.ac.cn (J.Y.); zhengxf@ccxida.com (X.Z.); zhanran23@mails.ucas.ac.cn (R.Z.); chenyufeng21@mails.ucas.ac.cn (Y.C.); cheny@ccxida.com (Y.C.); maoxy@ccxida.com (X.M.)
[2] University of Chinese Academy of Sciences, Beijing 100049, China
[3] Changchun Cedar Electronics Technology Co., Ltd., Changchun 130103, China; caoh@ccxida.com
* Correspondence: wangy@ccxida.com

Abstract

RGB channel response differences and model prediction bias limit joint grayscale luminance and chromaticity calibration in passive-matrix (PM) Mini-LED displays. A method combining local response modeling and output residual correction is therefore proposed. A forward model constructed from single-channel and equal-RGB-code responses is used to optimize a baseline compensation mapping allowing separate RGB drive-code adjustments. At five baseline compensation operating points, residuals are calculated as the differences between simulated outputs and model predictions evaluated at the same RGB triplet. These residuals are interpolated along the gray-level axis to update luminance and chromaticity predictions before reoptimizing the mapping. Numerical evaluation based on measured base-response data shows that, over 250 gray levels excluded from residual sampling in the original scenario, joint correction reduces the mean full-scale-normalized absolute luminance error from 0.2885% to 0.1028% and the mean chromaticity deviation $\Delta u'v'$ from 0.002823 to 0.001126 relative to the baseline mapping. Compared with residual correction using existing equal-RGB-code responses, these metrics decrease by a further 20.1% and 8.1%, respectively. Both advantages persist across 30 numerical recalibration runs in the original scenario. However, in scenario S1 with stronger candidate-code-dependent deviations, joint correction produces a higher mean luminance error than the baseline, while retaining a lower mean chromaticity deviation. The results indicate that sparse residual feedback can improve calibration at unsampled gray levels when sampled residuals adequately represent prediction bias within the candidate domain. Independent measurements at non-equal RGB triplets are still needed to validate physical calibration performance.

Keywords: Mini-LED; passive-matrix driving; gray-axis calibration; local response model; RGB compensation; residual correction

Check for updates

Academic Editor: Yahya Moubarak Meziani

Received: 18 September 2026
Revised: 28 October 2026
Accepted: 3 November 2026
Published: 6 November 2026

Copyright: © 2026 by the authors. Licensee MDPI, Basel, Switzerland. This article is an open access article distributed under the terms and conditions of the Creative Commons Attribution (CC BY) license.

1. Introduction

Mini-LEDs offer high luminance, long operational lifetimes, and flexible integration options, supporting applications in both emissive displays and liquid crystal display backlights [1,2]. In emissive display systems, pixel-driving schemes and grayscale control strategies directly affect luminance modulation, grayscale reproduction, and display uniformity [3]. Differences in the emission characteristics and driving conditions of RGB devices

can cause their relative contributions to vary with the input gray level, thereby affecting the luminance and chromaticity of the combined output [4,5]. Grayscale calibration therefore requires consideration of both target luminance reproduction and chromaticity consistency along the gray axis.

In RGB display systems, equal-code inputs, for which $R = G = B$, are commonly used to define a nominal gray axis. However, identical input codes do not imply identical normalized electro-optical responses across the three channels. When gamma correction or luminance matching is performed along the equal-code trajectory, all three channels share a single adjustment variable. Once the common code is selected, the output chromaticity is also determined. Previous studies have improved display output through gamma correction and RGB channel driving control [6,7]. For Micro-LED displays, grayscale control and luminance compensation have been integrated into display control systems [8], while iterative correction based on output measurements has been used to improve pixel luminance uniformity [9]. These studies provide a basis for implementing display calibration. For joint calibration along the gray axis, separate adjustment of the RGB drive codes is needed when the equal-code response cannot simultaneously satisfy the target luminance and reference chromaticity.

Solving for RGB compensation codes using a display response model is an established approach to joint luminance and chromaticity control. Early studies of display characterization established relationships between input codes and output color using channel responses and additivity assumptions [10]. Nonlinear channel transformations combined with a color transformation matrix subsequently formed the basis of classical display characterization methods [11,12]. To account for the response characteristics of devices such as liquid crystal displays, later studies incorporated variations in channel chromaticity and interactions among channels [13,14]. Nonlinear RGB-to-XYZ mappings provide greater flexibility in representing the input–output relationship [15]. In color device calibration, two-dimensional transformations have also been used to provide additional control beyond independent channel correction [16].

As characterization methods have developed, sampling distribution and model structure have become important factors affecting prediction accuracy. Colantoni et al. combined an adaptive training set with polyharmonic spline interpolation to construct a display color characterization model [17]. Poljicak et al. used optimized radial basis functions to model the color responses of mobile displays [18]. More recent work has compared machine learning methods across different display technologies, considering both prediction accuracy and model interpretability [19]. For gray-axis calibration, the required outputs are RGB compensation codes near each target gray level, allowing the model application and search domain to be restricted accordingly. Piecewise models that account for variations in channel chromaticity and local characterization methods provide a basis for this approach [20,21].

Restricting the candidate domain, however, does not eliminate model prediction errors. Black-level treatment affects display characterization accuracy [22], and an additive approximation based on single-channel responses may not fully describe the output under combined RGB driving. Such errors affect the evaluation of candidate codes and can cause the selected compensation codes to produce outputs that deviate from the target response. Previous studies have employed linear, nonlinear, and hybrid search algorithms to determine input codes that satisfy target luminance and chromaticity [23]. Automated sampling and compensation mechanisms have also been combined to improve calibration accuracy at low luminance levels [24]. For gray-axis calibration with existing base-response data, correcting prediction errors using a small number of representative compensation operating points offers a feasible way to limit additional sampling.

To address this problem, this study investigates a joint grayscale calibration method for PM-driven Mini-LED displays based on local response modeling and output residuals evaluated at the same RGB triplets. First, a local forward model is constructed from single-channel and equal-RGB-code responses. A baseline compensation mapping that allows separate adjustment of the RGB codes is then obtained under target luminance, fixed reference chromaticity, and drive-code constraints. Luminance and chromaticity residuals are subsequently constructed from simulated outputs at a small number of baseline compensation RGB triplets and interpolated along the target gray-level axis to update the forward predictions. The compensation mapping is then solved again. In this formulation, the base model describes the relative responses among candidate codes, while the gray-level-dependent residuals compensate for local prediction bias.

Using the measured base-response data, four approaches are evaluated: baseline mapping, correction using residuals derived from existing equal-RGB-code responses, five-point luminance-only residual correction, and five-point joint residual correction. Numerical evaluation is performed at gray levels excluded from residual sampling to compare the resulting luminance and chromaticity errors. Holdout tests over contiguous gray-level intervals are used to assess interpolation accuracy along the base-response trajectories. Repeated numerical recalibration and different deviation scenarios are further used to examine the effects and applicability of residual correction across gray-level intervals.

2. Materials and Methods

2.1. Overall Calibration Framework

The proposed method takes the target gray level as its input and returns the corresponding RGB drive codes. The calibration procedure consists of four stages: base-response characterization, local model construction, baseline mapping optimization, and residual correction. Figure 1 presents the overall workflow.

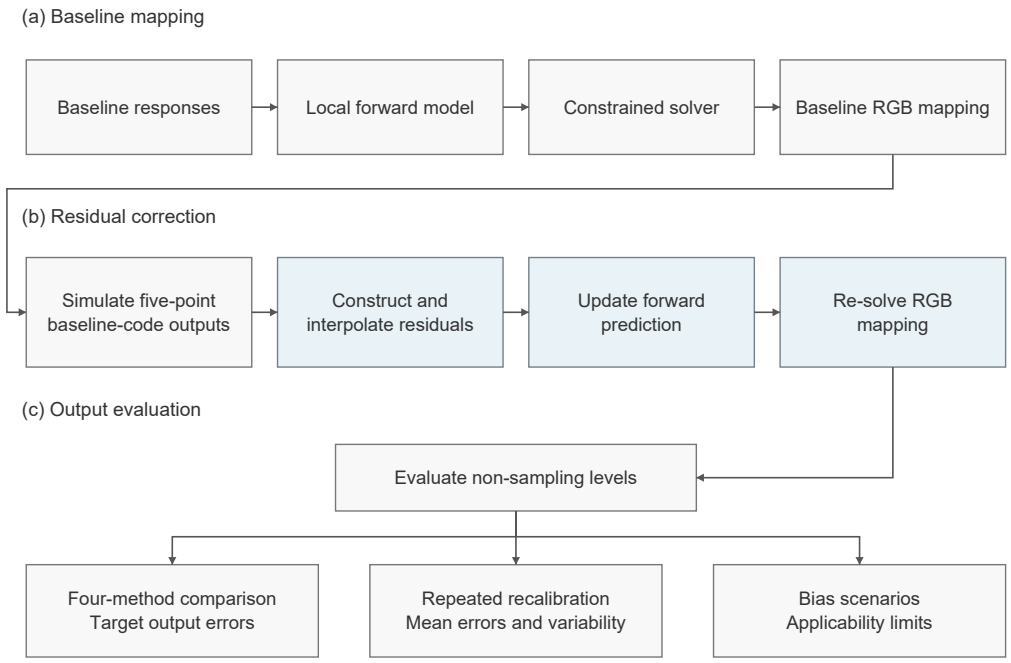


Figure 1. Overall workflow of joint grayscale luminance and chromaticity calibration.

A local forward model is first constructed from the individual R, G, and B channel responses and the equal-RGB-code response. The baseline compensation mapping is then ob-

tained using the target luminance, a fixed reference chromaticity, and drive-code constraints. At selected gray levels, simulated outputs are generated at the baseline compensation RGB triplets, and residuals are calculated relative to the predictions at those same triplets. The residuals are interpolated along the gray-level axis to update the forward predictions, after which the compensation mapping is solved again. Calibration performance is evaluated at gray levels excluded from residual sampling.

Throughout this study, an equal-RGB-code input refers to $R = G = B$, whereas an output and a prediction evaluated at the same RGB triplet may correspond to unequal channel codes. The residuals update the forward predictions, and the RGB drive codes are subsequently determined by solving the mapping optimization problem.

2.2. Base-Response Characterization

The base-response data were obtained from a P1.25 full-color Mini-LED display unit with integrated packaging, operated using PM driving and a 1/60 scan configuration. The original measurements were performed using a UP427 luminance/colorimeter (Konica Minolta (China) Investment Ltd., Shanghai, China) with uniform full-field test patterns. The measurement axis was aligned with the center of the active display area, and the ambient temperature was 24 °C. The display specifications and measurement conditions are summarized in Table 1. Figure 2 shows the display unit and measurement configuration.

Table 1. Display specifications and base-response measurement conditions.

Item	Specification
Display unit	PM-driven P1.25 full-color Mini-LED display with integrated packaging
Effective resolution	480 × 270 pixels
Active display area	600 × 337.5 mm
Pixel pitch	1.25 mm
Driving mode	1/60-scan constant-current driving
Column driver	ICND1065S
Measured refresh rate	2280 Hz
Input code range	0–255
Measurement instrument	UP427 luminance/colorimeter
Measured quantities	CIE XYZ tristimulus values, luminance Y, and CIE 1976 UCS chromaticity coordinates (u', v')
Test patterns	Uniform full-field patterns with single-channel and equal-RGB-code inputs
Measurement alignment	Instrument optical axis aligned with the center of the active display area
Ambient temperature	24 °C
Base-response acquisition	Four input sequences: $(g,0,0)$, $(0,g,0)$, $(0,0,g)$, and (g,g,g); 256 code levels per sequence, yielding 1024 response records

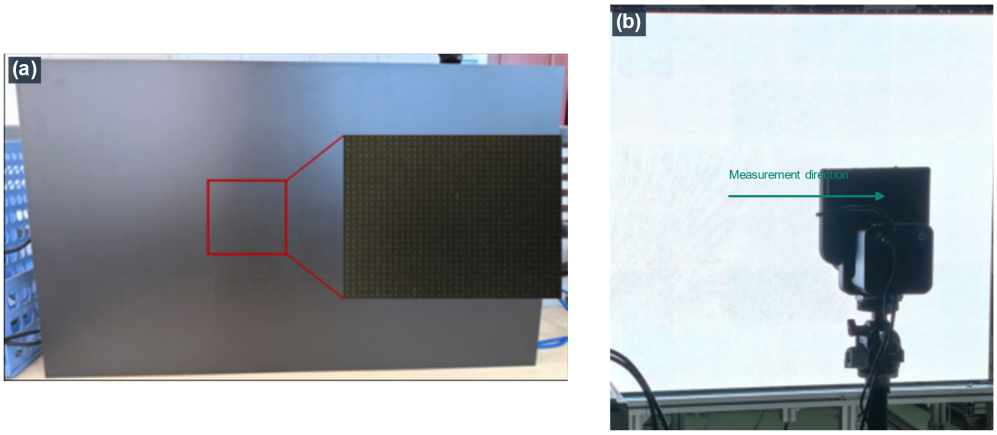


Figure 2. Mini-LED display unit and measurement configuration. (**a**) Display unit and local LED-array view. (**b**) Measurement arrangement, showing the instrument and measurement axis.

To characterize the luminance and chromaticity responses along the equal-RGB-code gray axis and in its neighborhood, CIE XYZ tristimulus values were measured for the individual R, G, and B channels and for equal-RGB-code inputs [25]. The four input sequences are defined as

$$(R, G, B) = (g, 0, 0), \quad (0, g, 0), \quad (0, 0, g), \quad (g, g, g). \tag{1}$$

The measured tristimulus vector for an equal-RGB-code input is denoted by $\mathbf{P}_W(g)$. The subscript W identifies the combined equal-RGB-code response and does not denote a white subpixel in an RGBW display.

Each input sequence covers all integer codes from $g = 0$ to 255, yielding 1024 base-response records. The single-channel responses are used to calculate the tristimulus increments of the individual primaries. The equal-RGB-code response is used to determine the black level, target luminance range, reference chromaticity, and candidate-domain center, and to construct the comparison method based on existing equal-RGB-code residuals.

Figure 3 presents the single-channel and equal-RGB-code luminance responses. In Figure 3a, the independent variable is the input code of the individual channel. In Figure 3b, the equal-RGB-code response is plotted against the common input code, whereas the target curve is plotted against the target gray level. Both use the same 0–255 scale for comparison.

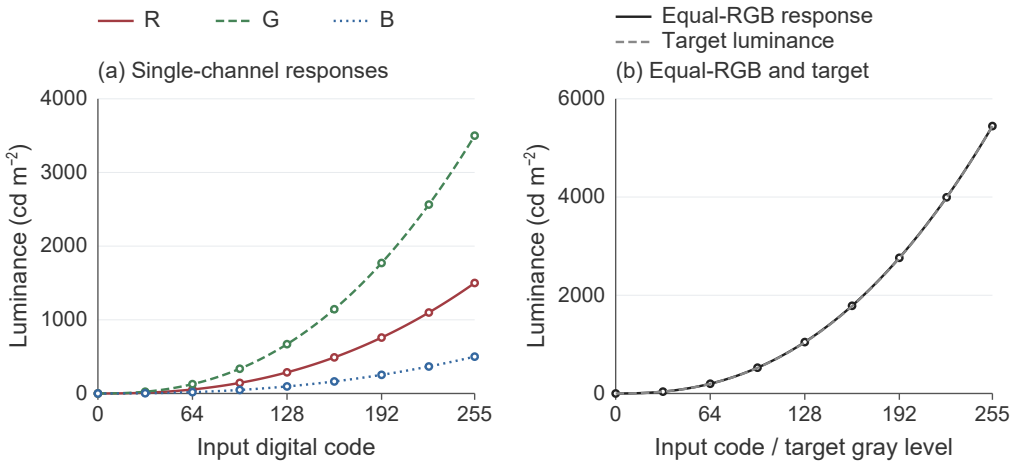


Figure 3. Measured base luminance responses. (**a**) Individual R, G, and B channel responses. (**b**) Equal-RGB-code response and target luminance curve.

2.3. Local Response Model near the Gray Axis

Let $\mathbf{P}_i(g) = [X_i(g), Y_i(g), Z_i(g)]^{\mathrm{T}}$ denote the measured tristimulus vector of primary channel $i \in \{R, G, B\}$ at input code g. The channel increment is defined by subtracting the zero-code output of the corresponding single-channel sequence:

$$\Delta\mathbf{P}_i(g) = \mathbf{P}_i(g) - \mathbf{P}_i(0). \tag{2}$$

A candidate RGB drive-code vector is denoted by $\mathbf{d} = [d_R, d_G, d_B]^{\mathrm{T}}$. Within the neighborhood of the equal-RGB-code gray axis, its tristimulus values are predicted using an additive approximation of the single-channel increments [10,13]:

$$\hat{\mathbf{P}}(\mathbf{d}) = \mathbf{P}_W(0) + \sum_{i \in \{R,G,B\}} \Delta\mathbf{P}_i(d_i). \tag{3}$$

Equation (3) uses the measured zero-code equal-RGB output as a common baseline and adds the response increment of each primary relative to its zero-code output. This

formulation avoids counting the black-level output more than once. The model describes relative luminance and chromaticity differences among local candidate codes, with its application restricted to the candidate domain near the equal-RGB-code gray axis.

The predicted luminance $\hat{Y}(\mathbf{d})$ is the Y component of $\hat{\mathbf{P}}(\mathbf{d})$. The chromaticity of the combined output is expressed in CIE 1976 UCS coordinates [25]:

$$\hat{u}' = \frac{4\hat{X}}{\hat{X} + 15\hat{Y} + 3\hat{Z}}, \qquad \hat{v}' = \frac{9\hat{Y}}{\hat{X} + 15\hat{Y} + 3\hat{Z}}. \tag{4}$$

Here, $\hat{X}$, $\hat{Y}$, and $\hat{Z}$ are the predicted tristimulus values. Equations (3) and (4) provide the predicted luminance and chromaticity for each candidate RGB triplet.

2.4. Target Response and Baseline Compensation Mapping

The target luminance at gray level g is defined using a gamma function that retains the residual luminance at zero input:

$$Y_T(g) = Y_W(0) + [Y_W(255) - Y_W(0)]\left(\frac{g}{255}\right)^{\gamma}. \tag{5}$$

Here, $Y_W(0)$ and $Y_W(255)$ are the measured luminances of the original equal-RGB-code input at zero and maximum code, respectively, and γ specifies the target grayscale curve. This definition determines the target dynamic range from the measured maximum-code luminance while retaining the actual black-level output of the display.

The reference chromaticity is obtained from the high-gray-level portion of the original equal-RGB-code response. Averaging the measured CIE 1976 UCS coordinates over g = 192–255 gives

$$u'_{\mathrm{ref}} = 0.195415, \qquad v'_{\mathrm{ref}} = 0.449820.$$

These values define a chromaticity reference for the display unit at high gray levels, rather than a standard white point or a prescribed correlated color temperature.

For each target gray level, the code $q_0(g)$ whose measured equal-RGB-code luminance is closest to $Y_T(g)$ is selected. The triplet $[q_0(g), q_0(g), q_0(g)]^{\mathrm{T}}$ is used as the initial drive-code vector for local search. It defines the candidate-domain center and is not directly used as the final compensation code.

Let the local candidate domain be denoted by $\Omega(g)$. For each channel $i \in \{R, G, B\}$, candidate codes satisfy

$$|d_i - q_0(g)| \le h, \qquad 0 \le d_i \le 255, \qquad \max_{i,j} |d_i - d_j| \le \delta.$$

All channel drive codes are integers. The parameter h limits the maximum deviation of an individual channel from the initial code, while δ limits the code difference between channels. This study uses $h = 6$ and $\delta = 10$.

The constrained baseline RGB mapping is solved in ascending order of target gray level. The original zero-code input is retained at $g = 0$. For nonzero gray levels, the baseline compensation code is defined as

$$\begin{aligned} \mathbf{d}_0^*(g) = \arg\min_{\mathbf{d}\in\Omega(g)} \Bigg\{ & \lambda_Y \left[\frac{\hat{Y}(\mathbf{d}) - Y_T(g)}{Y_W(255) - Y_W(0)} \right]^2 \\ & + \lambda_C \left[\left(\hat{u}'(\mathbf{d}) - u'_{\mathrm{ref}}\right)^2 + \left(\hat{v}'(\mathbf{d}) - v'_{\mathrm{ref}}\right)^2 \right] \\ & + \lambda_S \left\| \frac{\mathbf{d} - \mathbf{d}_0^*(g-1)}{255} \right\|_2^2 \Bigg\}. \end{aligned} \tag{6}$$

The weights λ_Y, λ_C, and λ_S correspond to the luminance error, chromaticity deviation, and drive-code continuity terms, respectively. The continuity term penalizes abrupt changes

in drive codes between adjacent target gray levels. Candidate codes must also satisfy the constraint on nondecreasing predicted luminance:

$$\hat{Y}(\mathbf{d}) \geq \hat{Y}[\mathbf{d}_0^*(g-1)] - \varepsilon_Y,$$

where ε_Y is the permitted luminance decrease.

The target gamma is set to $\gamma = 2.4$. The weights are $\lambda_Y = 1.0$, $\lambda_C = 1.0$, and $\lambda_S = 0.03$, and the luminance tolerance is $\varepsilon_Y = 0$. At each target gray level, the candidate with the minimum objective value among those satisfying the predicted-luminance constraint is selected. Candidates are ordered lexicographically by their R, G, and B codes; the first candidate is selected when computed objective values are equal. If no feasible candidate exists, the gray level is recorded and the current mapping optimization is terminated. The same solution rules are used for the baseline and residual-corrected mappings.

2.5. Mapping Correction Using Output Residuals at the Same RGB Triplets

To reduce prediction bias in the local model, simulated outputs are generated at the baseline compensation RGB triplets corresponding to the residual-sampling set

$$\mathcal{A} = \{16, 48, 96, 160, 224\}.$$

Five outputs are generated at each operating point, and the luminance and two chromaticity components are averaged separately:

$$\mathbf{z}_m[\mathbf{d}_0^*(g_a)] = \frac{1}{5}\sum_{k=1}^{5} \mathbf{z}_{m,k}[\mathbf{d}_0^*(g_a)].$$

Here, k indexes the five simulated outputs, and the subscript m denotes the output used in the residual calculation. The chromaticity components are obtained by averaging the five u' and v' coordinates separately.

Let $\mathbf{z} = [Y, u', v']^{\mathrm{T}}$ denote the luminance–chromaticity output vector, and let $\hat{\mathbf{z}}(\mathbf{d})$ denote the baseline prediction. The sampled residual, interpolated residual, and corrected prediction are defined as

$$\begin{aligned} \mathbf{r}(g_a) &= \mathbf{z}_m[\mathbf{d}_0^*(g_a)] - \hat{\mathbf{z}}[\mathbf{d}_0^*(g_a)], \\ \tilde{\mathbf{r}}(g) &= \mathcal{J}_g\{\mathbf{r}(g_a) \mid g_a \in \mathcal{A}\}, \\ \tilde{\mathbf{z}}(\mathbf{d}, g) &= \hat{\mathbf{z}}(\mathbf{d}) + \tilde{\mathbf{r}}(g). \end{aligned} \tag{7}$$

The operator $\mathcal{J}_g\{\cdot\}$ denotes piecewise linear interpolation. Linear interpolation is used between adjacent sampled gray levels. For nonzero gray levels outside the sampled range, the residual at the nearest endpoint is used. No residual correction is applied at zero gray level.

For a given target gray level g, $\tilde{\mathbf{r}}(g)$ is applied as a common correction to all candidates within $\Omega(g)$. The base model describes relative responses among candidate codes, while the gray-level-dependent residual compensates for local prediction bias. This approach reduces reliance on characterization of the full RGB combination space.

The baseline prediction components in Equation (6) are replaced by the corrected components, and the continuity term uses the corrected solution at the preceding gray level, $\mathbf{d}_{\mathcal{A}}^*(g-1)$. The corrected predicted-luminance constraint is

$$\tilde{Y}(\mathbf{d}, g) \geq \tilde{Y}[\mathbf{d}_{\mathcal{A}}^*(g-1), g-1] - \varepsilon_Y.$$

The right-hand side uses the predicted luminance at the preceding gray level with that level's own residual correction. Initialization at zero gray level uses the uncorrected predicted luminance. The optimization is solved again with the same target response, candidate domain, and weights to obtain the residual-corrected mapping $\mathbf{d}_{\mathcal{A}}^*(g)$.

2.6. Comparison Methods and Evaluation Procedure

Four methods are compared. Method A uses the baseline mapping. Method B constructs residuals from the existing equal-RGB-code responses. Method C corrects only the luminance component of the five-point residuals, whereas Method D corrects luminance and both chromaticity components. All four methods use the same target response, candidate domain, objective weights, and constraints. Additional sampling is counted by the number of residual operating points; Methods C and D each use five sampled gray levels.

For Method B, the difference between the measured response and the baseline prediction is calculated at the equal-code center $q_0(g)$. Let $\mathbf{z}_W(q)$ denote the luminance–chromaticity vector converted from $\mathbf{P}_W(q)$. The residual and corrected prediction are

$$\mathbf{r}_B(g) = \mathbf{z}_W[q_0(g)] - \hat{\mathbf{z}}\left[(q_0(g), q_0(g), q_0(g))^{\mathrm{T}}\right],$$
$$\tilde{\mathbf{z}}_B(\mathbf{d}, g) = \hat{\mathbf{z}}(\mathbf{d}) + \mathbf{r}_B(g).$$

This correction is constructed in the Y, u', v' space, with the correction at zero gray level set to zero. Methods C and D share the same five-point output records and interpolation results. Method C sets both chromaticity residual components to zero, while Method D retains all three components, allowing the effects of luminance-only and joint correction to be compared.

The single-channel and equal-RGB-code base responses are taken from existing measurements. Outputs for residual sampling, mapping evaluation, and repeated recalibration are generated using the numerical models in Appendix A. The original scenario, S0, combines the baseline prediction, the existing equal-RGB-code deviation, and a prescribed signed code-difference term, reproducing the measured tristimulus responses at equal-RGB-code inputs. The models define controlled deviation scenarios for evaluating residual correction. Within each scenario, all methods use the same output relationship, whose expected value is determined solely by the RGB drive codes.

After conversion from XYZ to Y, u', v', independent zero-mean Gaussian perturbations are added to the three components. The luminance standard deviation is

$$\sigma_Y = 0.04 + 0.0004Y \qquad (\mathrm{cd\,m^{-2}}).$$

The standard deviation of each chromaticity coordinate is 0.00004. Five outputs are generated at each operating point.

Luminance error and chromaticity deviation are calculated using a fixed luminance dynamic range and a fixed reference chromaticity. Chromaticity deviation is expressed as the Euclidean distance in the CIE 1976 UCS plane [25]:

$$E_Y(g) = \left|\frac{Y_m(g) - Y_T(g)}{Y_W(255) - Y_W(0)}\right| \times 100\%, \tag{8}$$

$$\Delta u'v'(g) = \sqrt{\left[u'_m(g) - u'_{\mathrm{ref}}\right]^2 + \left[v'_m(g) - v'_{\mathrm{ref}}\right]^2}. \tag{9}$$

In Equations (8) and (9), $Y_m(g)$, $u'_m(g)$, and $v'_m(g)$ denote the components of an individual simulated output, with the repetition index omitted for brevity. At each target gray level, errors are calculated separately for the five outputs and then averaged.

The evaluation set is

$$\mathcal{G} = \{1, \ldots, 255\} \setminus \mathcal{A},$$

which contains 250 gray levels. The mean and 95th percentile (P95) are calculated across the per-gray-level mean errors. Percentiles are computed using linear interpolation. Identical RGB triplets selected by different methods at the same target gray level share the same output records. The number of luminance decreases is counted from strict decreases in the mean output luminance between successive evaluated gray levels in ascending order.

To assess low-gray-level performance, the absolute relative luminance error and mean absolute luminance deviation are additionally calculated as

$$E_{Y,\mathrm{rel}}(g) = \frac{100\%}{N}\sum_{k=1}^{N}\frac{|Y_{m,k}(g) - Y_T(g)|}{Y_T(g)},$$
$$E_{Y,\mathrm{abs}}(g) = \frac{1}{N}\sum_{k=1}^{N}|Y_{m,k}(g) - Y_T(g)|, \qquad N = 5. \tag{10}$$

Both metrics use the same evaluation set $\mathcal{G}$, without additional exclusion of low-gray-level points or a lower bound on the normalization denominator. Results are summarized over g = 1–85, 86–170, and 171–255, containing 83, 83, and 84 evaluation levels, respectively. Table A4 reports the mean, P95, and maximum relative errors, together with the mean absolute luminance deviations, for the single S0 run underlying Table 2.

Table 2. Calibration results of the four methods over 250 gray levels excluded from residual sampling in the first S0 run.

Method	Additional Sampled Levels	Mean E_Y (%)	P95 E_Y (%)	Mean $\Delta u'v'$	P95 $\Delta u'v'$	Luminance Decreases
A: Baseline	0	0.288466	0.786224	0.002823	0.005014	10
B: Equal-code	0	0.128771	0.429041	0.001225	0.003881	0
C: Luminance-only	5	0.087868	0.194899	0.002870	0.004427	7
D: Joint	5	0.102849	0.265316	0.001126	0.003615	7

The original equal-RGB-code input, $\mathbf{d}(g) = (g, g, g)^{\mathrm{T}}$, is also included as a reference for comparing the original gray axis with the compensation mappings. This comparison fixes the mappings obtained in the first S0 run and uses expected outputs without evaluation perturbations. The same 250 gray levels and error definitions are used, and the results are reported in Table A2.

To examine performance under different deviation conditions, two additional scenarios are constructed from S0: S1 introduces candidate-code-dependent deviations, and S2 introduces local nonlinear deviations. S1 tests the transferability of residual corrections when deviations vary with the drive codes, while S2 examines the ability of sparse sampling to represent local variations along the gray-level axis. Both additional terms vanish at equal-RGB-code inputs.

Thirty recalibration runs are performed for each scenario. In each run, the five-point outputs are regenerated and the mappings for Methods C and D are solved again, while the mappings for Methods A and B remain fixed. Separate random streams are used for calibration and evaluation. The mean error and P95 are calculated within each run, after which their means and sample standard deviations across runs are determined.

For S1 and S2, interval-wise mean errors are calculated within each run over the same three gray-level intervals. Their means and sample standard deviations are then determined across the 30 numerical recalibration runs. The single-run S0 results and the 30-run S1/S2 statistics are reported separately.

A one-factor sensitivity analysis is performed with $\lambda_C = 0.5,\ 1.0,\ 2.0$. The luminance and continuity weights remain fixed at $\lambda_Y = 1$ and $\lambda_S = 0.03$, respectively, to examine the effect of chromaticity weighting under otherwise unchanged objective settings. All four mappings are reoptimized using the fixed residuals from the first S0 calibration, with the same candidate domain and constraints. Evaluation uses unperturbed expected outputs over $\mathcal{G}$. The original weights were specified before this analysis. Results are reported in Table A5.

The interpolation used to reconstruct the base responses is evaluated separately using holdout tests over contiguous gray-level intervals. Gray levels 8–15, 64–79, 128–143, and

208–223 are simultaneously removed from each of the four response trajectories. Piecewise linear interpolation of the XYZ components is performed using the remaining 200 points, and prediction errors are evaluated at the 56 held-out points.

3. Results and Discussion

3.1. Effects of Residual Correction on Gray-Axis Luminance and Chromaticity Errors

Table 2 summarizes the calibration results of the four methods in the original scenario, S0. The baseline mapping yields a mean luminance error of 0.288466% and a mean chromaticity deviation of 0.002823. Incorporating residuals derived from the existing equal-RGB-code responses reduces these values to 0.128771% and 0.001225, respectively. This improvement indicates that the combined equal-RGB-code response contains calibration information that is not fully represented by the baseline additive model.

Channel additivity is commonly used in display characterization, whereas departures from this assumption can affect prediction accuracy [10,13]. In the present numerical model, the equal-RGB-code residual incorporates the combined-response deviation into the forward prediction, accounting for the improvement from Method A to Method B.

Five-point joint residual correction further reduces the overall errors. Relative to the baseline mapping, the mean luminance error and mean chromaticity deviation decrease by 64.3% and 60.1%, respectively. Relative to the equal-RGB-code residual method, the corresponding mean errors decrease by 20.1% and 8.1%, while their P95 values decrease by 38.2% and 6.9%. Baseline compensation codes generally lie away from the equal-RGB-code trajectory. Calculating residuals from simulated outputs at these operating points therefore helps compensate for local prediction bias that the equal-RGB-code response alone does not fully describe.

Figure 4 divides the gray-level range into three intervals: 1–85, 86–170, and 171–255. After excluding the residual-sampling levels, these intervals contain 83, 83, and 84 evaluation points, respectively. The bar heights represent the mean errors within each interval, and Table 3 reports the corresponding P95 and maximum errors.

In the low-gray-level interval, joint correction reduces both mean luminance error and mean chromaticity deviation relative to the equal-RGB-code residual method. In the middle interval, it reduces luminance error but slightly increases chromaticity deviation. In the high-gray-level interval, the equal-RGB-code residual method provides lower luminance error, whereas joint correction provides lower chromaticity deviation. The calibration benefits thus vary across the gray-level range and reflect different trade-offs between luminance and chromaticity.

The original equal-RGB-code input further illustrates this trade-off. In Table A2, its mean luminance error is 0.067167%, lower than the 0.101954% obtained with joint correction, whereas joint correction yields lower mean and P95 chromaticity deviations. Relative to the original gray axis, the primary benefit of the proposed method is therefore improved chromaticity consistency. Residual correction reduces the luminance cost introduced by the baseline compensation mapping.

3.2. Roles of Luminance and Chromaticity Residuals and Their Trade-Off

Figure 5 shows the residuals at the five sampled operating points. The luminance residuals are negative at all five points, ranging from $-0.013865\,\mathrm{cd\,m^{-2}}$ at $g = 16$ to $-34.220686\,\mathrm{cd\,m^{-2}}$ at $g = 224$. These values indicate that the baseline model overestimates the output luminance at the sampled compensation codes. The corresponding u' residuals are positive and the v' residuals are negative. Their magnitudes increase across the sampled gray levels, indicating gray-level-dependent bias in both luminance and chromaticity predictions.

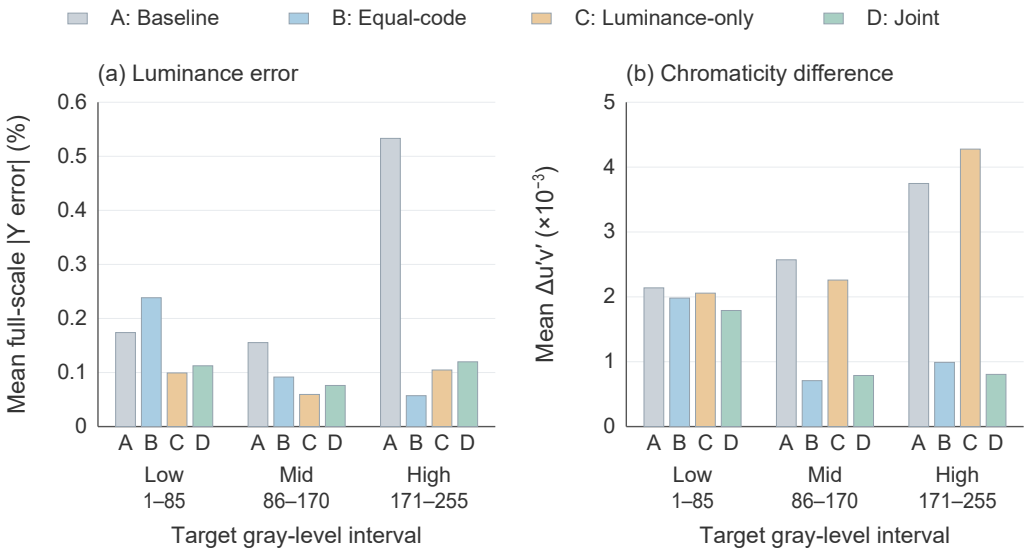


Figure 4. Mean errors over three gray-level intervals for a single calibration run in scenario S0. (**a**) Mean full-scale-normalized absolute luminance error, normalized by the equal-RGB-code luminance dynamic range, $Y_W(255) - Y_W(0) = 5444.9532\,\mathrm{cd\,m^{-2}}$. (**b**) Mean chromaticity deviation from the fixed reference $(u'_{\mathrm{ref}}, v'_{\mathrm{ref}}) = (0.195415, 0.449820)$.

Table 3. P95 and maximum errors within the three gray-level intervals.

Interval	Method	Gray Levels	Luminance P95 (%)	Maximum Luminance Error (%)	Chromaticity P95	Maximum Chromaticity Deviation
Low: 1–85	A	83	0.284023	0.313974	0.004117	0.005852
	B	83	0.509355	0.574262	0.004673	0.005852
	C	83	0.193080	0.201179	0.004106	0.005852
	D	83	0.221840	0.249245	0.004108	0.005852
Mid: 86–170	A	83	0.278353	0.288005	0.003651	0.003709
	B	83	0.143733	0.151643	0.001029	0.001047
	C	83	0.169990	0.188300	0.004311	0.004373
	D	83	0.125574	0.135903	0.001029	0.001047
High: 171–255	A	84	0.862779	1.209093	0.005032	0.005063
	B	84	0.095909	0.106303	0.001315	0.001394
	C	84	0.288831	0.605033	0.004441	0.004490
	D	84	0.311833	0.333387	0.001168	0.001250

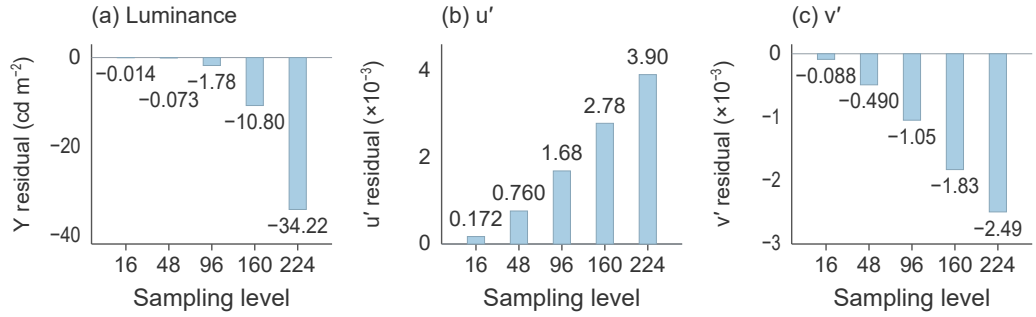


Figure 5. Signed residuals at the five sampled operating points in the first calibration run of scenario S0. (**a**) Luminance residual in $\mathrm{cd\,m^{-2}}$. (**b**) u' residual. (**c**) v' residual. Residuals are defined as the mean simulated output minus the prediction at the same baseline compensation RGB triplet.

Luminance-only correction yields a mean luminance error of 0.087868% and a luminance P95 of 0.194899%, both the lowest among the four methods. Its mean chromaticity deviation, however, is 0.002870. Including the two chromaticity residual components reduces

the mean chromaticity deviation to 0.001126, a decrease of 60.8% relative to luminance-only correction. The chromaticity P95 decreases by 18.3%, while the mean luminance error increases by approximately 17%. These results indicate that the luminance residual primarily improves luminance matching, whereas the chromaticity residuals alter the selection of candidate codes to bring the compensated output closer to the fixed reference chromaticity.

Table A4 supplements the full-scale-normalized metric with target-relative and absolute luminance errors for the same single S0 run. Over $g = 1$–85, the mean absolute relative luminance errors of Methods A–D are 103.029%, 144.257%, 95.136%, and 96.652%, respectively. Method D has a lower mean relative error than Methods A and B, while Method C gives the lowest value. The large relative errors indicate that low-gray-level luminance reproduction remains inaccurate despite the reduction in full-scale-normalized error.

At $g = 32$, the target luminance is $37.3866\,\mathrm{cd}\cdot\mathrm{m}^{-2}$. The mean absolute luminance deviation of Method D is $6.7499\,\mathrm{cd}\cdot\mathrm{m}^{-2}$, corresponding to a relative error of 18.05%. Full-scale normalization describes deviations relative to the display luminance range, whereas target-relative and absolute errors characterize reproduction at individual gray levels. These metrics therefore provide complementary descriptions of calibration performance.

Table A5 presents the chromaticity-weight sensitivity results under fixed S0 calibration data. For Method D, increasing λ_C from 0.5 to 2.0 reduces the mean chromaticity deviation from 0.001242 to 0.000941, while the mean full-scale-normalized luminance error changes from 0.099901% to 0.100868%. Method C retains a lower mean luminance error than Method D at all three tested weights. The results show that chromaticity weighting affects the balance between luminance matching and proximity to the reference chromaticity. The chromaticity metric describes distance in the CIE 1976 UCS plane [25], while luminance accuracy is evaluated separately. These fixed-residual results complement the five-output statistics in Table 2.

3.3. Numerical Robustness and Applicability

Table A1 presents the results of the holdout tests over contiguous gray-level intervals. For the equal-RGB-code response, the mean absolute luminance prediction error is $4.810\,\mathrm{cd\,m}^{-2}$, and the mean chromaticity prediction distance between predicted and held-out outputs at the same input codes is 0.000503. Within the held-out interval $g = 8$–15, the chromaticity prediction distance is 0.003385, higher than those in the other held-out intervals. This result indicates greater sensitivity of low-gray-level chromaticity to base-response reconstruction.

Table 4 and Figure 6 summarize the 30 recalibration runs under the three output scenarios. Table 4 reports the averages across runs of the within-run mean errors and P95 values. The error bars in Figure 6 represent sample standard deviations across runs.

In S0, joint correction yields a mean luminance error of $(0.104049 \pm 0.001704)\%$ and a mean chromaticity deviation of 0.001128 ± 0.000013. In all 30 runs, its mean luminance error, luminance P95, mean chromaticity deviation, and chromaticity P95 are lower than those of the equal-RGB-code residual method. The improvements in this scenario are therefore maintained under repeated sampling and mapping optimization.

In S1, joint correction yields a mean luminance error of 0.327218%, exceeding the 0.168140% of the baseline mapping and the 0.116081% of the equal-RGB-code residual method. Its mean chromaticity deviation is 0.001215, lower than the baseline value of 0.002264 but slightly higher than that of the equal-RGB-code residual method. Candidate-code-dependent deviations increase the variation in residuals among different drive-code combinations. Consequently, corrections obtained at the baseline compensation codes become less representative of the operating points selected after reoptimization, leading to increased luminance error.

Table 4. Results of 30 recalibration runs for the four methods under different output scenarios.

Scenario	Method	Mean Luminance Error (%)	Luminance P95 (%)	Mean Chromaticity Deviation	Chromaticity P95
S0	A	0.288497	0.789808	0.002821	0.005015
	B	0.128048	0.429081	0.001224	0.003891
	C	0.088729	0.195514	0.002869	0.004427
	D	0.104049	0.262677	0.001128	0.003622
S1	A	0.168140	0.385739	0.002264	0.003689
	B	0.116081	0.432182	0.001201	0.003849
	C	0.146822	0.280920	0.002178	0.003437
	D	0.327218	1.131818	0.001215	0.003577
S2	A	0.475431	2.364177	0.003143	0.007942
	B	0.228558	0.469374	0.001519	0.003845
	C	0.412758	1.581953	0.003125	0.007317
	D	0.164400	0.532692	0.001236	0.003817

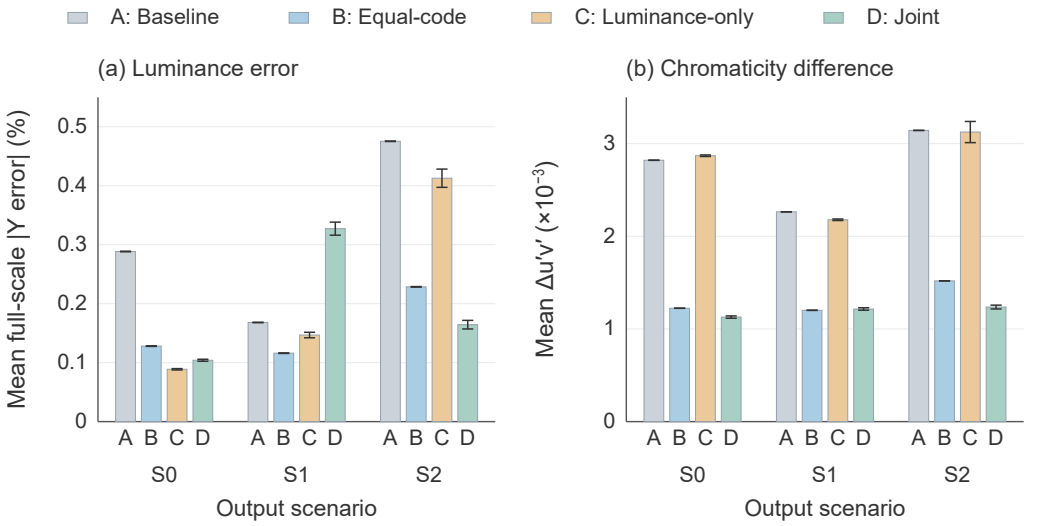


Figure 6. Comparison of errors under repeated recalibration in three output scenarios. (**a**) Mean full-scale-normalized absolute luminance error. (**b**) Mean chromaticity deviation. Bar heights represent the means across 30 runs, and error bars indicate sample standard deviations across runs.

In S2, the mean luminance error and mean chromaticity deviation of joint correction are 0.164400% and 0.001236, respectively, both lower than those of the equal-RGB-code residual method. Its luminance P95, however, is 0.532692%, higher than the comparison value of 0.469374%. Joint correction therefore reduces the mean errors, while larger luminance deviations remain at some gray levels.

Figure 7 further compares the methods across gray-level intervals. In S1, Method C has the lowest mean luminance error in the low interval, whereas Method B has the lowest mean luminance error in the middle and high intervals. Method D has the lowest mean chromaticity deviation in the low and middle intervals, and Method B has the lowest value in the high interval. In the middle interval, Method D reduces mean chromaticity deviation by 25.9% relative to Method B, with a 77.1% increase in mean luminance error. The high interval contributes most to the luminance deterioration of Method D: its mean error is 0.7360%, compared with 0.2287% for Method A and 0.0382% for Method B.

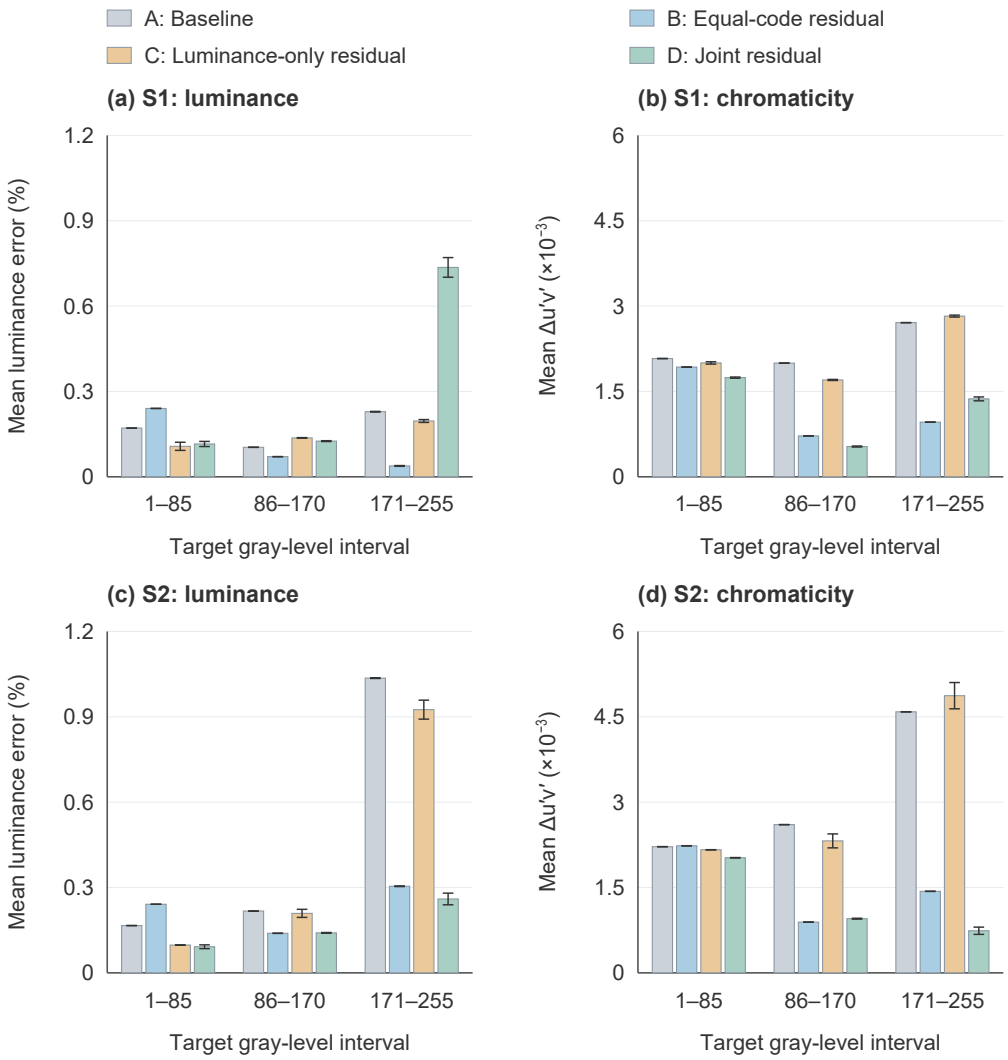


Figure 7. Interval-wise calibration errors across 30 numerical recalibration runs in S1 and S2. (**a**) S1 luminance error. (**b**) S1 chromaticity deviation. (**c**) S2 luminance error. (**d**) S2 chromaticity deviation. The intervals 1–85, 86–170, and 171–255 contain 83, 83, and 84 evaluation levels, respectively, after excluding the residual-sampling levels. Within each run, errors are first averaged over five outputs at each gray level and then over the evaluation levels in each interval. Bar heights and error bars represent the means and sample standard deviations of the interval averages across runs.

In S2, Method D has the lowest mean luminance error and mean chromaticity deviation in the low and high intervals, whereas Method B has the lowest values for both metrics in the middle interval. In the high interval, Method D reduces mean luminance error and mean chromaticity deviation by 14.7% and 48.4%, respectively, relative to Method B. These interval comparisons are based on averages across 30 numerical recalibration runs, whereas Figure 4 presents the single-run S0 results.

Sampling distribution and local model structure affect display characterization accuracy [17,21]. In S2, the imposed sinusoidal component depends on the mean RGB code q, rather than directly on the target gray level g. As shown in Table A3, the last three sampled operating points lie at or near the same zero-crossing phase. At the first sampling point, the RGB codes are equal, so the additional S2 term vanishes. The five operating points therefore provide limited coverage of the periodic component and may miss deviations between samples. This phase distribution indicates potential sensitivity to sampling position; it does

not establish resonance or the optimality of the selected sampling levels. The S2 results correspond to the tested period and phase.

The predicted luminance and unperturbed expected luminance of all mappings remain nondecreasing. The decreases in mean output luminance reported in Table 2 occur where adjacent evaluated gray levels select identical RGB codes and arise from independently generated output perturbations. These counts describe local fluctuations in the perturbed output sequences and should be distinguished from violations of the predicted-luminance monotonicity constraint.

The results indicate that a common residual correction is applicable when prediction bias varies only weakly among candidate operating points and can be approximated along the gray-level axis using a small number of samples. This study uses numerical output relationships constructed from measured base responses. The main limitation is the absence of independent measurements at non-equal RGB triplets. The base-response holdout tests assess interpolation accuracy along the measured trajectories, but do not validate the assumed deviations at non-equal RGB inputs. Negative tristimulus components occur at some unselected low-code combinations, whereas all evaluated mapping outputs satisfy the nonnegativity check. The applicability of the numerical model is therefore restricted to the evaluated operating points. Independent measurements at the compensation codes and neighboring RGB triplets are needed to establish the calibration performance on the display unit.

4. Conclusions

This study proposes a joint grayscale calibration method for PM-driven Mini-LED displays to address the effects of model prediction bias on compensation performance. The method combines local response modeling with output residuals evaluated at the same RGB triplets. Single-channel and equal-RGB-code base responses are used to obtain a compensation mapping that allows separate adjustment of the RGB codes. Luminance and chromaticity residuals calculated from simulated outputs at five baseline compensation operating points are interpolated along the gray-level axis to update the forward predictions, after which the mapping is solved again.

Numerical evaluation based on the measured base-response data shows that, in the single S0 run evaluated over 250 non-sampling gray levels, joint correction reduces the mean full-scale-normalized absolute luminance error from 0.288466% to 0.102849% and the mean chromaticity deviation from 0.002823 to 0.001126 relative to the baseline mapping. Compared with the equal-RGB-code residual method, the two metrics decrease by a further 20.1% and 8.1%, respectively. Luminance-only correction achieves lower luminance error, whereas joint correction further improves chromaticity consistency. Comparison with the original equal-RGB-code input shows that this chromaticity improvement entails a luminance cost, while residual correction reduces the prediction-related errors introduced by the baseline mapping. The mean relative luminance error of joint correction remains 96.652% in the low-gray-level interval, indicating that accurate dark-level reproduction is not achieved under the tested configuration.

The mean luminance and chromaticity advantages over equal-RGB-code residual correction are maintained across 30 numerical recalibration runs in S0. The relative performance of the methods changes with the deviation scenario and gray-level interval. In S1, joint correction has a higher mean luminance error than the baseline mapping, 0.3272% versus 0.1681%, while retaining a lower mean chromaticity deviation. Method C has the lowest mean luminance error in the low interval, and Method B in the middle and high intervals. Method D has the lowest mean chromaticity deviation in the low and middle intervals, and Method B in the high interval. In S2, Method D has the lowest values for both mean

metrics in the low and high intervals, whereas Method B has the lowest values in the middle interval. These results indicate that sparse residual correction is effective when sampled residuals represent prediction bias at the operating points selected after reoptimization. The findings are based on numerical evaluation; independent measurements at non-equal RGB triplets are needed to validate physical calibration performance.

Author Contributions: Conceptualization, J.Y.; Methodology, J.Y. and H.C.; Software, J.Y.; Validation, H.C.; Investigation, R.Z.; Data Curation, Y.C. (Yufeng Chen); Writing—Original Draft Preparation, J.Y.; Writing—Review and Editing, Y.C. (Yu Chen); Visualization, J.Y.; Supervision, X.Z.; Project Administration, X.M.; Funding Acquisition, Y.C. (Yufeng Chen) and Y.W.; Resources, Y.C. (Yufeng Chen) and Y.W. All authors have read and agreed to the published version of the manuscript.

Funding: National Science and Technology Major Project of the 15th Five-Year Plan (2025ZD0615803); Cooperation Project between the Chinese Academy of Sciences and the Changchun Municipal Government (24SH04).

Data Availability Statement: Data underlying the results presented in this paper are not publicly available at this time but may be obtained from the authors upon reasonable request.

Acknowledgments: The authors thank Deju Huang of Jilin Institute of Chemical Technology for valuable advice and the critical reading of the manuscript.

Conflicts of Interest: Authors Jinhuan Yu, Xifeng Zheng, Yufeng Chen, Xinyue Mao, Hui Cao, Yang Wang and Yu Chen were employed by the company Changchun Cedar Electronics Technology Co., Ltd. The remaining author declares that the research was conducted in the absence of any commercial or financial relationships that could be construed as a potential conflict of interest.

Appendix A. Numerical Output Models and Supplementary Validation

Appendix A.1. Original Output Model

The numerical output models are constructed from measured base responses to evaluate residual correction under controlled deviations. The additional code-dependent terms define hypothetical deviation scenarios for examining the influence of prediction bias on calibration performance.

Let $\hat{\mathbf{P}}(\mathbf{d})$ denote the baseline prediction. The mean input code q, normalization factor s, and coefficient η are defined as

$$q = \frac{d_R + d_G + d_B}{3}, \qquad s = \max(q, 1), \qquad \eta = \frac{\min(d_R, d_G, d_B)}{s}.$$

The deviation between the existing equal-RGB-code response and the baseline prediction is

$$\mathbf{e}(j) = \mathbf{P}_W(j) - \hat{\mathbf{P}}\left([j, j, j]^{\mathsf{T}}\right), \qquad j = 0, \ldots, 255.$$

Interpolation is performed separately for the three XYZ components to obtain $\mathbf{e}(q)$. The original numerical output model is then defined as

$$\begin{aligned}\mathbf{F}_0(\mathbf{d}) &= \hat{\mathbf{P}}(\mathbf{d}) + \eta\,\mathbf{e}(q) \\ &\quad + \hat{\mathbf{P}}(\mathbf{d}) \odot \left\{ 0.01\eta \left[\frac{d_R - d_G}{s} \begin{pmatrix} 0.3 \\ 1 \\ -0.2 \end{pmatrix} + \frac{d_B - d_G}{s} \begin{pmatrix} -0.2 \\ 0.1 \\ 1 \end{pmatrix} \right] \right\}. \end{aligned} \tag{A1}$$

Here, $\odot$ denotes element-wise multiplication. Equation (A1) uses the existing equal-RGB-code deviation $\mathbf{e}(q)$ to anchor the response and extends the model to unequal RGB codes through the channel-code difference terms and their coefficients. For nonzero equal-RGB-code inputs, $\eta = 1$ and both channel-code differences vanish, so the model reproduces the existing equal-RGB-code XYZ responses. At zero input, the baseline black level is retained.

The coefficient η controls the contribution of the additional terms in Equation (A1). It equals unity for nonzero equal-RGB-code inputs and becomes zero when any channel code is zero. The latter condition eliminates the terms multiplied by η in S0. The additional terms in S1 and S2 are defined separately and need not vanish under the same condition. The signed first-order code differences specify the direction of the imposed deviation with changes in relative channel codes. Both η and these code-difference terms are mathematical components of the test model, rather than identified physical load or channel-coupling parameters.

Appendix A.2. Deviation Scenarios

The candidate-dependent scenario S1 is defined as

$$\mathbf{F}_1(\mathbf{d}) = \mathbf{F}_0(\mathbf{d}) + \hat{\mathbf{P}}(\mathbf{d}) \odot \left\{ 0.03 \tanh\left(\frac{d_R - d_G}{6} \right) \tanh\left(\frac{d_B - d_G}{6} \right) \begin{pmatrix} 0.4 \\ 1 \\ -0.3 \end{pmatrix} \right\}. \tag{A2}$$

The locally nonlinear scenario S2 is defined as

$$\mathbf{F}_2(\mathbf{d}) = \mathbf{F}_0(\mathbf{d}) + \hat{\mathbf{P}}(\mathbf{d}) \odot \left\{ 0.03 \tanh\left(\frac{\max(\mathbf{d}) - \min(\mathbf{d})}{6} \right) \sin\left(\frac{2\pi q}{64} \right) \begin{pmatrix} 0.2 \\ 1 \\ -0.2 \end{pmatrix} \right\}. \tag{A3}$$

Scenario S1 introduces candidate-dependent deviations through the product of hyperbolic tangent functions of the channel-code differences. Scenario S2 introduces local nonlinear variation through a sinusoidal function of the mean input code. The coefficients 0.01 and 0.03 specify amplitudes relative to the baseline prediction, while the vector coefficients specify the relative directions of change in the XYZ components. The scale parameters 6 and 64 govern the dependence on channel-code differences and the variation with mean input code, respectively. These prescribed parameters define controlled numerical scenarios and are not fitted to independent non-equal-RGB measurements.

Appendix A.3. Supplementary Evaluation

Table A1 summarizes the prediction errors for held-out points along the four base-response trajectories. MAE and RMSE denote the mean absolute error and root mean square error, respectively. Chromaticity distances are calculated by converting the predicted XYZ values and the held-out XYZ values at the same RGB triplets to chromaticity coordinates. Luminance errors are normalized by the dynamic range determined from the retained endpoints of the equal-RGB-code response.

Table A1. Prediction errors for contiguous held-out gray-level intervals along the four base-response trajectories.

Response Trajectory	Held-Out Points	Luminance MAE ($cd\,m^{-2}$)	Luminance RMSE ($cd\,m^{-2}$)	Normalized Luminance MAE (%)	Mean Chromaticity Distance
R	56	1.330157	1.529034	0.024429	0.000839
G	56	3.105237	3.567726	0.057030	0.000407
B	56	0.443414	0.509657	0.008144	0.000649
Equal-RGB code	56	4.809737	5.520674	0.088334	0.000503

Table A2 compares the unperturbed expected outputs of the original equal-RGB-code input and the compensation mappings obtained in the first calibration run of S0. All methods

use the same 250 evaluation gray levels and error definitions, with their compensation mappings held fixed.

Table A2. Unperturbed output errors of the original equal-RGB-code input and the four compensation mappings in S0.

Method	Mean E_Y (%)	P95 E_Y (%)	Mean $\Delta u'v'$	P95 $\Delta u'v'$
Original equal-RGB-code input	0.067167	0.127609	0.004709	0.004134
A: Baseline	0.288338	0.790772	0.002820	0.005009
B: Equal-code	0.126549	0.429152	0.001222	0.003895
C: Luminance-only	0.087540	0.192970	0.002869	0.004427
D: Joint	0.101954	0.263366	0.001123	0.003621

The mean chromaticity deviation of the original equal-RGB-code input is affected by large deviations at very low gray levels. After additionally excluding gray levels 1–7, the mean chromaticity deviations over the remaining 243 evaluation gray levels are 0.001969, 0.002836, 0.001164, 0.002885, and 0.001089 for the original input and methods A–D, respectively. Joint correction still reduces the mean chromaticity deviation by approximately 44.7% relative to the original input, indicating that the chromaticity improvement is maintained over this adjusted evaluation range.

Appendix A.4. Sampling Phases in Scenario S2

The baseline compensation RGB triplets at the five residual-sampling levels are identical across the 30 S2 recalibration runs. Table A3 lists their mean input codes and phases for the period-64 sinusoidal component in Equation (A3). The phase is calculated as

$$\phi = 360^\circ \frac{q \bmod 64}{64}.$$

Table A3. Mean input codes and sinusoidal phases at the five residual-sampling operating points in S2.

g	Baseline RGB Triplet	q	ϕ (Degrees)	$\sin(2\pi q/64)$
16	(10, 10, 10)	10.000	56.250	0.8315
48	(46, 45, 46)	45.667	256.875	−0.9739
96	(97, 95, 96)	96.000	180.000	0.0000
160	(162, 158, 161)	160.333	181.875	−0.0327
224	(227, 221, 225)	224.333	181.875	−0.0327

The mean input codes are displayed to three decimal places. Phases and sine values are calculated using the unrounded q values obtained from the integer RGB triplets. The last three operating points lie at or near the same zero-crossing phase. At $g = 16$, the RGB codes are equal, and the amplitude factor $\tanh[(\max(\mathbf{d}) - \min(\mathbf{d}))/6]$ is zero. The sampling configuration therefore provides limited coverage of the periodic component and may miss deviations between operating points. This phase distribution indicates potential sensitivity to sampling position rather than established resonance. The analysis concerns the specified period and phase.

Appendix A.5. Repeated Calibration and Result Verification

For run r, the calibration and evaluation random seeds are $20260915 + 1000r$ and $20260916 + 1000r$, respectively, where $r = 0, \ldots, 29$. Methods C and D share the calibration records. Within the same scenario, run, and target gray level, identical RGB triplets share the same evaluation outputs. Variation between runs for methods A and B arises from

evaluation perturbations, whereas methods C and D also include mapping changes caused by calibration perturbations.

The first run of the original scenario corresponds to Table 2. All 360 sets of method-level statistics were recomputed from the saved individual output records. No solver failures occurred during the calculations.

Appendix A.6. Relative Luminance Errors and Weight Sensitivity

Table A4 reports the target-relative and absolute luminance errors for the single S0 run underlying Table 2. The metrics are calculated using Equation (10). Errors are first averaged over five outputs at each gray level and then summarized within each interval. The evaluation set excludes zero gray level and the five residual-sampling levels, leaving 83, 83, and 84 evaluation levels in the three intervals. Relative errors are expressed in percent, and absolute luminance deviations are expressed in cd · m^{-2}.

Table A4. Interval-wise relative and absolute luminance errors for the single S0 calibration run.

Interval	Method	n	Mean $E_{Y,\mathrm{rel}}$ (%)	P95 $E_{Y,\mathrm{rel}}$ (%)	Maximum $E_{Y,\mathrm{rel}}$ (%)	Mean $E_{Y,\mathrm{abs}}$
1–85	A	83	103.029	180.241	2881.816	9.470
	B	83	144.257	536.373	2881.816	12.980
	C	83	95.136	180.241	2881.816	5.404
	D	83	96.652	180.241	2881.816	6.123
86–170	A	83	0.833	2.691	2.854	8.459
	B	83	0.586	1.009	1.118	4.989
	C	83	0.253	0.553	0.568	3.237
	D	83	0.515	1.009	1.118	4.142
171–255	A	84	0.764	0.917	1.209	29.031
	B	84	0.099	0.193	0.236	3.113
	C	84	0.141	0.307	0.605	5.701
	D	84	0.175	0.331	0.362	6.524

Table A5 reports the one-factor chromaticity-weight analysis under fixed S0 calibration data. The luminance and continuity weights remain fixed at $\lambda_Y = 1$ and $\lambda_S = 0.03$. All four mappings are reoptimized using the fixed residuals from the first S0 calibration and the same candidate domain and constraints. Evaluation uses unperturbed expected outputs over the 250 non-sampling gray levels. These results are reported separately from the five-output statistics in Table 2.

Table A5. Chromaticity-weight sensitivity with fixed S0 calibration residuals and unperturbed expected outputs.

λ_C	Method	Mean E_Y (%)	P95 E_Y (%)	Mean $\Delta u'v'$	P95 $\Delta u'v'$
0.5	A	0.290049	0.814086	0.002431	0.003739
	B	0.104885	0.352239	0.001259	0.003895
	C	0.086486	0.259764	0.002149	0.004403
	D	0.099901	0.277618	0.001242	0.003739
1.0	A	0.288338	0.790772	0.002820	0.005009
	B	0.126549	0.429152	0.001222	0.003895
	C	0.087540	0.192970	0.002869	0.004427
	D	0.101954	0.263366	0.001123	0.003621
2.0	A	0.282202	0.790772	0.003014	0.005032
	B	0.168639	0.522484	0.000985	0.003848
	C	0.083464	0.185735	0.002940	0.004455
	D	0.100868	0.194789	0.000941	0.003131

References

1. Huang, Y.; Hsiang, E.-L.; Deng, M.-Y.; Wu, S.-T. Mini-LED, Micro-LED and OLED displays: Present status and future perspectives. *Light Sci. Appl.* **2020**, *9*, 105. [CrossRef] [PubMed]
2. Wu, T.; Sher, C.-W.; Lin, Y.; Lee, C.F.; Liang, S.; Lu, Y.; Huang Chen, S.W.; Guo, W.; Kuo, H.C.; Chen, Z. Mini-LED and micro-LED: Promising candidates for the next generation display technology. *Appl. Sci.* **2018**, *8*, 1557. [CrossRef]
3. Gao, H.; Zou, M.; Zhong, C.; Zhuang, J.; Lin, J.; Lu, Z.; Jiang, Z.; Lu, Y.; Chen, Z.; Guo, W. Advances in pixel driving technology for micro-LED displays. *Nanoscale* **2023**, *15*, 17232–17248. [CrossRef] [PubMed]
4. Guo, W.; Chen, N.; Lu, H.; Su, C.; Lin, Y.; Chen, G.; Lu, Y.; Zheng, L.; Peng, Z.; Kuo, H.C.; et al. The impact of luminous properties of red, green, and blue mini-LEDs on the color gamut. *IEEE Trans. Electron Devices* **2019**, *66*, 2263–2268. [CrossRef]
5. Steinel, T.; Wolf, M. 58-3: Invited Paper: Color uniformity of μLED displays: New color calibration concept for fast and accurate optical testing. *SID Symp. Dig. Tech. Pap.* **2021**, *52*, 822–825. [CrossRef]
6. Xiao, K.; Fu, C.; Karatzas, D.; Wuerger, S. Visual gamma correction for LCD displays. *Displays* **2011**, *32*, 17–23. [CrossRef]
7. Liu, S.-M.; Chou, Y.-C. Color calibration for a surrounding true-color LED display system by PWM controls. *IEEE Trans. Ind. Electron.* **2014**, *61*, 6244–6252. [CrossRef]
8. Chen, Y.; Zheng, X.; Cao, H.; Wang, Y.; Cheng, H.; Chen, J.; Huang, S.; Li, J.; Huang, D.; Chen, Y. High precision control system for Micro-LED displays. *Appl. Sci.* **2023**, *13*, 10601. [CrossRef]
9. Hsia, S.-C.; Wang, S.-H.; Yang, N.-H. Position calibration and pixel correction for uneven brightness Micro LED display. *IET Circuits Devices Syst.* **2025**, *2025*, 4243080. [CrossRef]
10. Brainard, D.H. Calibration of a computer controlled color monitor. *Color Res. Appl.* **1989**, *14*, 23–34. [CrossRef]
11. Berns, R.S.; Motta, R.J.; Gorzynski, M.E. CRT colorimetry. Part I: Theory and practice. *Color Res. Appl.* **1993**, *18*, 299–314. [CrossRef]
12. Berns, R.S. Methods for characterizing CRT displays. *Displays* **1996**, *16*, 173–182. [CrossRef]
13. Day, E.A.; Taplin, L.; Berns, R.S. Colorimetric characterization of a computer-controlled liquid crystal display. *Color Res. Appl.* **2004**, *29*, 365–373. [CrossRef]
14. Tamura, N.; Tsumura, N.; Miyake, Y. Masking model for accurate colorimetric characterization of LCD. *J. Soc. Inf. Disp.* **2003**, *11*, 333–339. [CrossRef]
15. Xiong, W.; Funt, B. Nonlinear RGB-to-XYZ mapping for device calibration. *Color Imaging Conf.* **2005**, *13*, 200–204. [CrossRef]
16. Bala, R.; Sharma, G.; Monga, V.; Van de Capelle, J.-P. Two-dimensional transforms for device color correction and calibration. *IEEE Trans. Image Process.* **2005**, *14*, 1172–1186. [CrossRef] [PubMed]
17. Colantoni, P.; Thomas, J.-B.; Hardeberg, J.Y. High-end colorimetric display characterization using an adaptive training set. *J. Soc. Inf. Disp.* **2011**, *19*, 520–530. [CrossRef]
18. Poljicak, A.; Dolic, J.; Pibernik, J. An optimized Radial Basis Function model for color characterization of a mobile device display. *Displays* **2016**, *41*, 61–68. [CrossRef]
19. Almutairi, K.; Morillas, S.; Latorre-Carmona, P.; Dansoko, M.; Gacto, M.J. A comparative analysis of machine learning methods for display characterization. *Displays* **2024**, *85*, 102849. [CrossRef]
20. Thomas, J.-B.; Hardeberg, J.Y.; Foucherot, I.; Gouton, P. The PLVC display color characterization model revisited. *Color Res. Appl.* **2008**, *33*, 449–460. [CrossRef]
21. Zou, W.; Xu, H.; Gong, R. Efficient and accurate local model for colorimetric characterization of liquid-crystal displays. *Opt. Lett.* **2012**, *37*, 31–33. [CrossRef] [PubMed]
22. Berns, R.S.; Fernandez, S.R.; Taplin, L. Estimating black-level emissions of computer-controlled displays. *Color Res. Appl.* **2003**, *28*, 379–383. [CrossRef]
23. Ban, H.; Yamamoto, H. A non-device-specific approach to display characterization based on linear, nonlinear, and hybrid search algorithms. *J. Vis.* **2013**, *13*, 20. [CrossRef] [PubMed]
24. Li, Y.-M.; Meng, W.; Tsai, C.-Y.; Lee, T.-X. A polynomial regression-based calibration method for enhancing chromaticity and luminance accuracy at low luminance levels of LCDs with automated sampling and compensation mechanisms. *Displays* **2026**, *92*, 103336. [CrossRef]
25. CIE. *Colorimetry*, 4th ed.; CIE 015:2018; International Commission on Illumination: Vienna, Austria, 2018. [CrossRef]

Disclaimer/Publisher's Note: The statements, opinions and data contained in all publications are solely those of the individual author(s) and contributor(s) and not of MDPI and/or the editor(s). MDPI and/or the editor(s) disclaim responsibility for any injury to people or property resulting from any ideas, methods, instructions or products referred to in the content.